Applied Nanoscience (2019) 9:1319–1331
https://doi.org/10.1007/s13204-018-00944-9

ORIGINAL ARTICLE

Investigation of cyclic voltammetry, impedance spectroscopy and electrical properties of thermally exfoliated biomass-synthesized graphene

Rabina Bhujel[1] · Sadhna Rai[1] · Bibhu P. Swain[2]

Received: 27 October 2018 / Accepted: 19 December 2018 / Published online: 7 January 2019

Abstract
In this paper we have reported the synthesis of graphene by a novel and facile thermal exfoliation process of *Allium cepa* (Onion) and was characterized by scanning electron microscopy, atomic force microscopy, X-ray diffraction, Raman spectroscopy, and X-ray photoelectron spectroscopy to investigate the morphological and structural properties and chemical networks present on it. The AFM and SEM images revealed the formation of thin strip-like layered structure of graphene with the thickness of 1.1 nm. The electrochemical properties of graphene were characterized by cyclic voltammeter, impedance spectroscopy, Tafel plot, Nyquist plot, Bode plot, and voltage-dependent impedance using 0.5 M H_2SO_4 electrolyte as an illustrative standard material. The cyclic voltammetric curve of graphene electrodes determined a quasi-reversible electrochemical behavior under linear diffusion control square shape at higher process temperature. The ratio of atomic % C-to-O varied from 7.57 to 24.04 indicating a decrease in the oxygen content for the graphene processed at higher temperature. The areal capacitance and voltage-dependent impedance varied from 8.59×10^{-5} to 18.8×10^{-5} F/cm^2 and 15.79 to 7.7 Ohm, respectively, with the process temperature varying from 600 to 1000 °C. The corrosion potential (E_{corr}) and corrosion current density (I_{corr}) values are −0.12 V and −9.1A/cm^2, respectively, for the graphene processed at 1000 °C.

Keywords Graphene · Cyclic voltammetry · Tafel plot · Nyquist plot · Bode plot

Introduction

Supercapacitors are capacitors with high energy densities, long cycle life, short charging time and high power density than conventional capacitors. Recently, carbonaceous nanomaterials consisting of activated carbon, carbon nanotube and graphene have attracted increasing attention for supercapacitors (Hao and Li 2013; Pan et al. 2010; Q.Ke 2016; EI-Kady et al. 2016; Lin et al. 2017; Pal et al. 2018). Among these carbonaceous materials, graphene which is a two-dimensional sheet of sp^2-hybridized carbon and has a unique structure and superior properties such as high surface area, excellent mechanical strength, and low electrical resistivity. Among many methods, the synthesis of graphene including the chemical route where graphene oxide (GO) can be prepared via chemical process, namely via Hummers method and can be reduced to obtain reduced graphene oxide (rGO) which is decorated mostly with hydroxyl groups on the surface and a small amount of carboxyl and carbonyl groups at the sheet edges (Zaaba et al. 2017). Moreover, quality graphene is synthesized by chemical vapour deposition (CVD) and mechanical exfoliation for its application in various fields (Park et al. 2010; Novoselov et al. 2004). However, the CVD-grown and mechanically exfoliated graphene have some limitations in mass production and substrate support requirement. Therefore, the biomass synthesis of graphene using natural products is an excellent alternative to produce large-scale graphene in a simple and cost-effective way (Shams et al. 2015). Supriya et al. (2016) investigated impedance spectroscopy and electrical properties of $CoFe_2$–rGO nanocomposite for its possible application as an anode material. Singal et al. (2017) investigated electrochemical impedance

✉ Bibhu P. Swain
bibhuprasad.swain@gmail.com; bpswain@nitmanipur.ac.in

[1] Centre for Materials Science and Nanotechnology, Sikkim Manipal Institute of Technology, Sikkim Manipal University, Majhitar, India

[2] Department of Physics, National Institute of Technology, Manipur, Langol, Imphal, Manipur 795004, India

analysis of biofunctionalized conducting polymer-modified graphene-CNTs nanocomposite for protein detection. Phan et al. (2016) investigated the electrochemical activity of PANi–TiO_2–GO composites synthesized by chemical method. Wang et al. (2017) utilized a thin film of graphene on the surface of sodium metal to produce highly stable sodium metal anodes for energy storage devices. Skryshevsky et al. (2015) investigated impedance spectroscopy of single graphene layer for ethanol and acetone gas sensor. Yoon et al. (2017) investigated impedance spectroscopy of GO and modeled the equivalent circuit of GO solutions. Bonanni et al. (2013) investigated high-resolution impedance spectroscopy to distinguish between oxidized and reduced graphene platforms. Marcelina et al. (2017) studied characteristic of rGO as supercapacitors' electrode materials and estimated specific capacitance of 6.53 mF g^{-1} as measured from 4 mg ml^{-1}RGO thin film at scan rate of 25 mVs^{-1}. Portales et al. (2018) investigated cyclic voltammetry and impedance spectroscopy analysis for graphene-modified solid-state electrode transducers. Akgul et al. (2016) characterized graphene oxide produced by Hummers method and its supercapacitor applications. Balasubramanian et al. (2018) investigated electrochemical analysis of graphene/Mo_9Se_{11} nanocomposites towards energy storage application. Yan et al. (2014) fabricated a two-dimensional atomic crystal-layered materials including H–BN and graphene as an effective protective layer for 2D layer−Li−Cu sandwich structure to improve the lithium metal anodes. Uri et al. (2014) investigated physicochemical characteristics of reduced graphene oxide-based Pt-nanoparticles conducting polymer nanocomposite film for immune sensor applications. Li et al. (2016) investigated one-step electrosynthesis of graphene oxide-doped polypyrrole nanocomposite as a nanointerface for electrochemical impedance detection of cell adhesion and proliferation using two approaches. Roy et al. (2015) investigated nitrogen-doped reduced graphene oxide-based Pt−TiO_2 nanocomposites for enhanced H_2 evolution. Jain et al. (2016) investigated apolyaniline/graphene oxide nanocomposite as a voltammetric sensor for electroanalytical detection of clonazepam.

The above research established by different researchers using graphene or graphene nanocomposite as an electrode is to evaluate the capacitance, corrosion potential, and impedance from electrochemical impedance and cycle voltammetry technique. However, our present paper aimed at (a) to investigate the capacitive property of graphene using cyclic voltammetry, (b) to investigate graphene as corrosion-protective materials as a possible application in corrosion resistance coating using Tafel plot, (c) to investigate frequency-dependent impedance of graphene electrode from Bode and Nyquist plot, and (d) voltage-dependent impedance and phase change of graphene produced at different temperature.

Experimental details

The extracted onion peels (scientific name *Allium cepa*) were used as a raw material for the synthesis of graphene. To remove the moisture from the collected onion peels, a 110 °C temperature was applied for 3 h in an oven. To perform the thermal exfoliation process in anaerobic condition, a silicon carbide resistance vacuum furnace (made: V.B. Ceramics) was used. During the heating process, Ar gas (IOLAR-I grade of BOC, India) was purged in the furnace to make an inert atmosphere. The successive quality production of graphene was achieved at the temperature 600–1000 °C at the ramp rate of 5 °C per minute to fix temperature and maintain the same for 2 h. The SEM characterization of graphene sample was done by JEOL, JSM 5510. The AFM image of graphene sample was obtained by Nanoscope III scanning probe microscope. The XPS spectroscopy was done using (VG ESCA-LABMK II with a Mg(K_α) X-ray (1253.6 eV) source and Raman characterization was done with the help of 532 nm laser at 1.5 mW power (WitecAlpha300 RS). The I–V characteristics of graphene samples were measured with the help of KEYSIGHTB2901A precession source/measure unit. Finally, the electrochemical properties of graphene samples were analyzed with the help of CH Instruments, Inc. (Electrochemical AnayzerCHI608E) using Ag/AgCl as the reference electrode, Pt wire as the counter electrode and graphene-coated glassy carbon electrode as the working electrode. The electrolytic solution contained 0.5MH_2SO_4 solution.

Results and discussion

Figure 1a and b shows the SEM and AFM images of graphene synthesized at the process temperature of 1000 °C. The SEM image shows a sheet-like transparent structure of graphene while the AFM image revealed the formation of thin stripe-like graphene structures. The formation of such graphene sheets is due to the breaking of various bonds present in the onion cells (cellulose) at higher temperature and the molecular rearrangement taking place, with the evolution of different organic functional groups and leaving behind a thin transparent sheet-like structure of graphene. The thickness of the sample was ~ 1.1 nm as obtained by the height profile diagram inset in the AFM image of graphene sample synthesized at 1000 °C. Moreover, the following equation was used to calculate the number of layers via AFM.

$$N = \frac{t_{\text{measured}} - 0.4}{0.335} \quad (1)$$

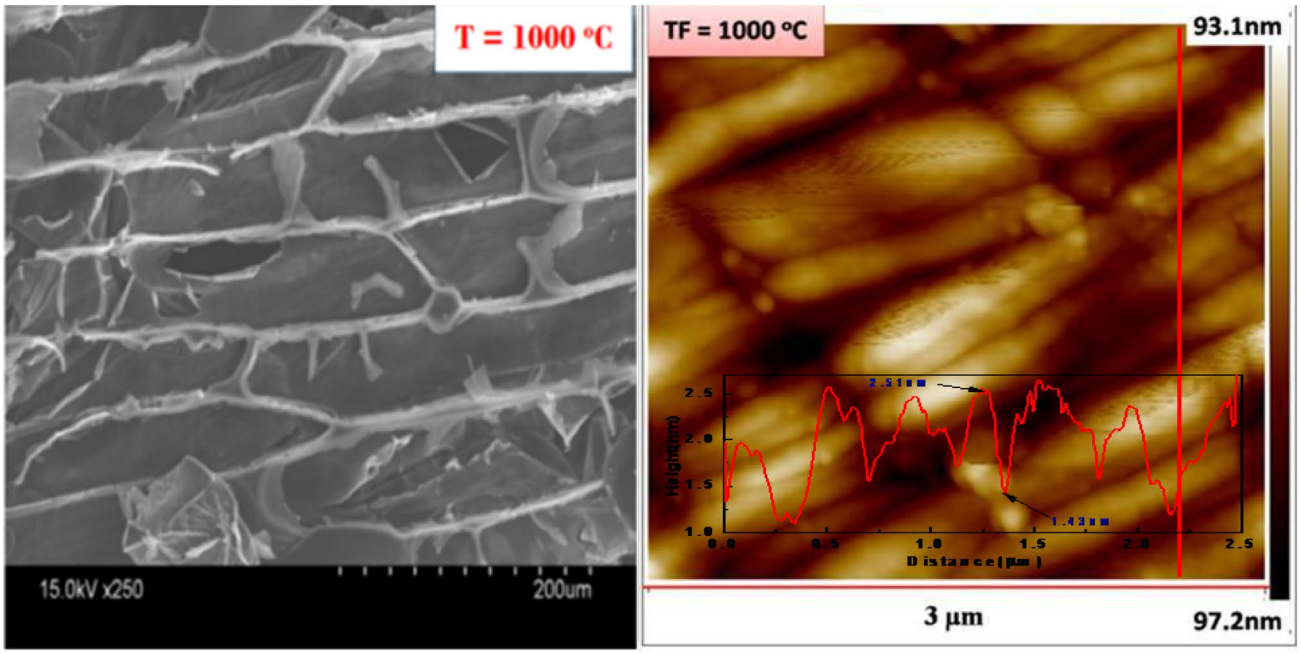

Fig. 1 **a** SEM and **b** AFM images of graphene samples synthesized at the process temperature of 1000 °C

where N is the number of layers, $t_{measured}$ is the measured thickness via AFM and 0.4 is the nominal value subtracted to account for increases in measured thickness related to substrate–graphene and graphene–tip interactions (Shearer et al. 2016). The above calculation revealed that the graphene sample processed at 1000 °C is bilayer in nature.

Figure 2a shows the Raman spectra of graphene processed at the temperature of 1000 °C. The asymmetric peak observed at 1000–2000 cm^{-1} corresponds to the first-order Raman peak, which arises as a result of the first-order phonon scattering in multilayered graphene structure. Figure 2b shows the second-order Raman peak of graphene samples in the range of 2300–3300 cm^{-1} confirming the formation of multilayered graphene structure. For the detailed analysis and better understanding, the first- and second-order Raman spectra of graphene samples were deconvoluted into six Lorentzian peaks arising at peak at 1150, 1350, 1583, 2588.3, 2734.1, and 2920.2 cm^{-1} corresponding to D*, D, G, G*, 2D and D + G or D + D', respectively. Bharathidasan et al. observed similar results for the graphene carbonaceous composites (Bharathidasan et al. 2016). The D peak arises by the LO phonon modes near the K point in the Brillouin Zone corresponding to the defect states in graphene layers and G peak arises at the Γ point in the Brillouin Zone for the in-plane vibration of sp^2-hybridized C atoms of the hexagonal C ring within the graphene sheets. Furthermore, the D* peak is attributed to LA phonon modes which arise due to the highly disordered morphology of sp^3-hybridized amorphous carbon structures, originated at the edges and holes of the graphene layers at the H-terminating edge of C=C chains. The second-order Raman band of graphene sample is observed for the symmetry allowed overtone of G band, which are useful for detecting the stacking order of graphene sheets in different graphene samples. The double resonant process of D (LO) phonons gives rise to 2D bands, whereas the D and G (LO) phonon resonance gives the D + G peak. The G* peak is attributed to the highly disordered morphology of sp^3-hybridized amorphous carbon structures. Moreover, the broadness and low intensity of the second-order Raman signature may be due to the presence of defect states or the multilayered structure of amorphous graphene sheets. The observation shows some similarity with the previously reported work by Johra and Gao et al. for the graphene sample (Johra et al. 2014; Gao et al. 2013). The major observations obtained from the deconvolution are.

1. Raman signature of G* shifts towards the higher frequency region (blue shift) from 1583 to 1584 cm^{-1}, which may be due to the decrease in the number of graphene layers at higher temperature.
2. The 2D band of all graphene samples is not sharp indicating the formation of multilayered graphene structure.
3. The peak intensity as well as the FWHM of D + G band is increased with increasing the process temperature indicating an increase in the number of disorders within

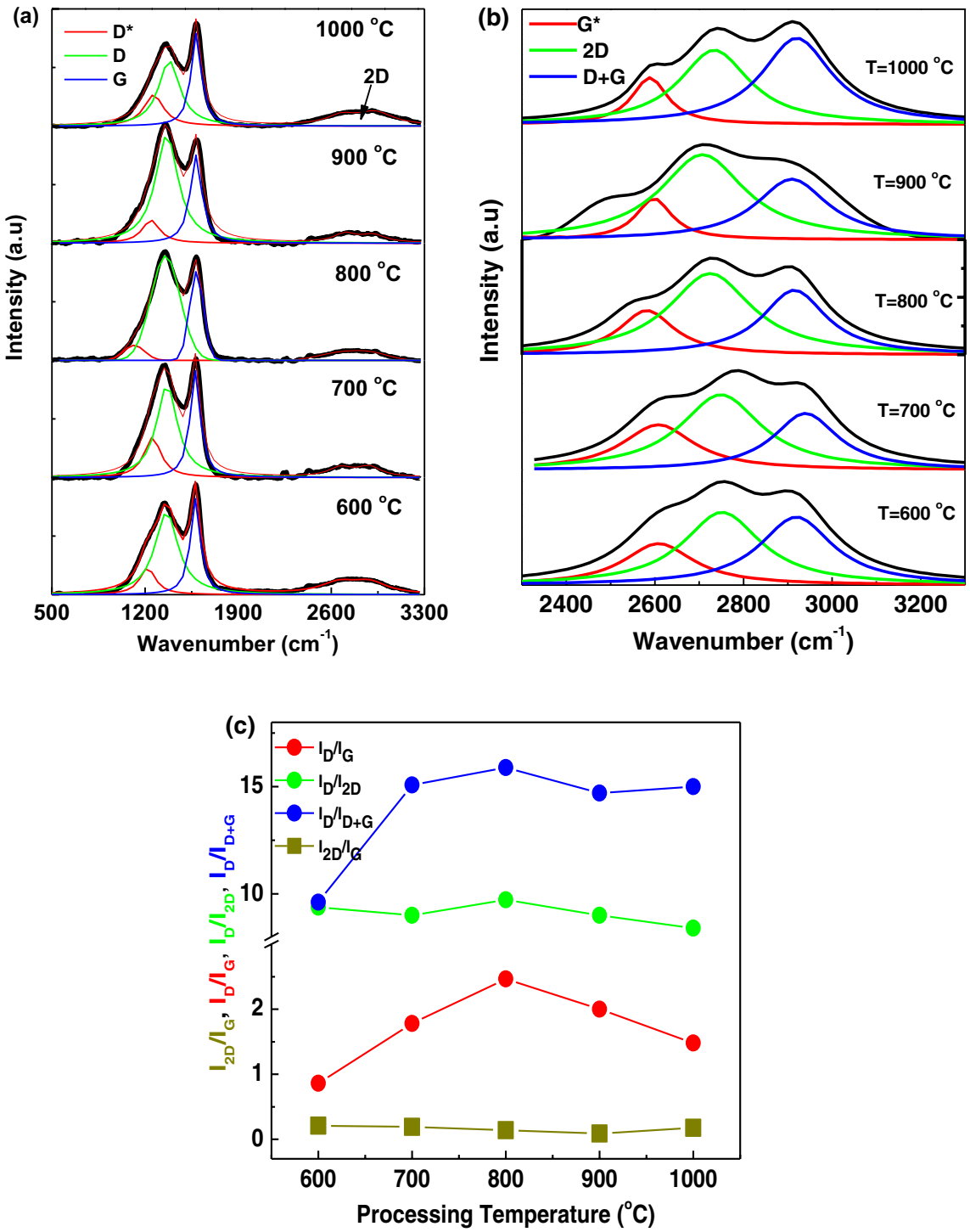

Fig. 2 **a** Full-scan Raman spectra with the deconvoluted first-order Raman peaks. **b** The deconvoluted second-order Raman peak of all the graphene samples synthesized by varying the process temperature from 600 to 1000°C

the graphene samples. From the as-obtained Raman spectra of the graphene samples processed at 600–1000 °C, the authors attempted to calculate the number of layers (n) using the formula.

$$\omega_G = 1581.6 + \frac{11}{1 + n^{1.6}} \quad (2)$$

where ω_G = G band position in wavenumber, n = number of layers. The calculated result showed that the number of

layers (n) in graphene samples varied from ~3 − 2 as the process temperature increased from 600 to 1000°C.(Wall 2011).

Figure 2c shows the intensity ratios of I_D/I_G, I_{2D}/I_G, I_D/I_{2D} and I_D/I_{D+G} of Raman parameters of graphene samples with the process temperature varying from 600 to 1000 °C. The following observations are obtained

1. The intensity ratio of I_D/I_G increases from 1.47 to 2.0 with the simultaneous decrease in I_{2D}/I_G from 0.21 to 0.17 for the process temperature increasing from 600 to 1000 °C. The increase in the I_D/I_G ratio and decrease in I_{2D}/I_G is due to the breaking of different bonds within the graphene layers indicating the loss of three dimensional ordering of C atoms which further leads to an increase in the number of defect states present in the graphene sheets (Andrea 2007). According to Tuinstra and Koenig $I_D/I_G = C(\lambda)/La$, where the coefficient C (514 nm) ~ 4.4 nm ($\lambda \equiv 2\pi c/\omega L$ is the excitation wavelength) and La is the crystal size (Tuinstra and Koenig 1970). Therefore, the greater the value of I_D/I_G ratio, smaller is the size of graphene cluster and hence more the number of disorders present in the graphene sheets. The ratio I_{2D}/I_G for high-quality (defect free) single-layer graphene is equal to 2. But in our case a slight decrease of I_{2D}/I_G ratio 0.21–0.17 with the increase in the process temperature is may be due to a decrease in the number of stacking order in multilayer graphene samples at higher process temperature.
2. The intensity ratio of I_D/I_{2D} decreases from 9.38 to 9 with the increasing process temperature. The I_D/I_{2D} ratio well explains the decrease in the edge disorders present in the graphene samples as well as the increased number of layers of graphene.
3. The intensity ratios of I_D/I_{D+G} increase from 9.6 to 14.7, with increasing the process temperature from 600 to 1000 °C. The I_D/I_{D+G} give an idea about the total number of C atoms with sp^2 out-phase disorder present within the graphene samples. The increase of I_D/I_{D+G} ratio indicates the increasing number of structural defects in graphene layers during the evolution of various volatile functional groups of the graphene layers at higher temperature.

Figure 3 Shows the XRD patterns of graphene samples synthesized by varying the process temperature from 600 to 1000 °C. The XRD diffraction patterns obtained at ~24.6° and ~44.7° with the corresponding planes of (002) and (100) indicated the formation of graphene sheets as reported earlier by Latif et al. for reduced graphene oxide (Latif and Merza 2016).Moreover, the broadness of the peak at ~24.6° confirms the formation of amorphous graphene. The full width at half maxima (FWHM) of XRD peaks varied from 6.5 to 8.4°, due to the variation in the ring structure ordering of graphene and

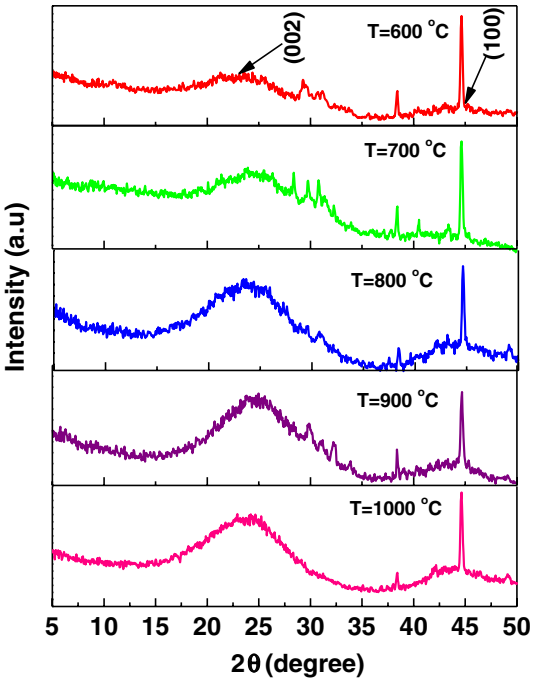

Fig. 3 XRD patterns of graphene samples by varying the process temperature from 600 to 1000 °C

increasing defect states with the temperature change. The calculated values of d spacing in graphene layers was observed to vary from 3.61 to 3.73 A° with the process temperature varying from 600 to 1000°Cas a result of the decrease in number of graphene layers at higher temperature. The number of layers present in graphene samples was further calculated using the formula.

$$n = \frac{D}{d} \tag{3}$$

where n = number of graphene layers, D = crystallite size and d = lattice spacing between the graphene layers. The estimated number of layers in graphene varied from 3.6 to 2.7 with the process temperature varying from 600 to 1000 °C as calculated using Eq. 3. This result shows similarity with the Raman results obtained using Eq. (2).

Figure 4a shows the XPS scan of graphene samples synthesized by varying the process temperature from 600 to 1000 °C. The core orbital binding energies for C(1 s) and O(1 s) are observed at 285.1 and 534.7eV, respectively, as earlier reported by Vijapur et al. (2017). The atomic percentage of C-to-O in the graphene sheets was calculated by applying the formula.

$$\text{Atomic } \% = \frac{\frac{A_i}{S_i}}{\sum \frac{A_i}{S_i}} \tag{4}$$

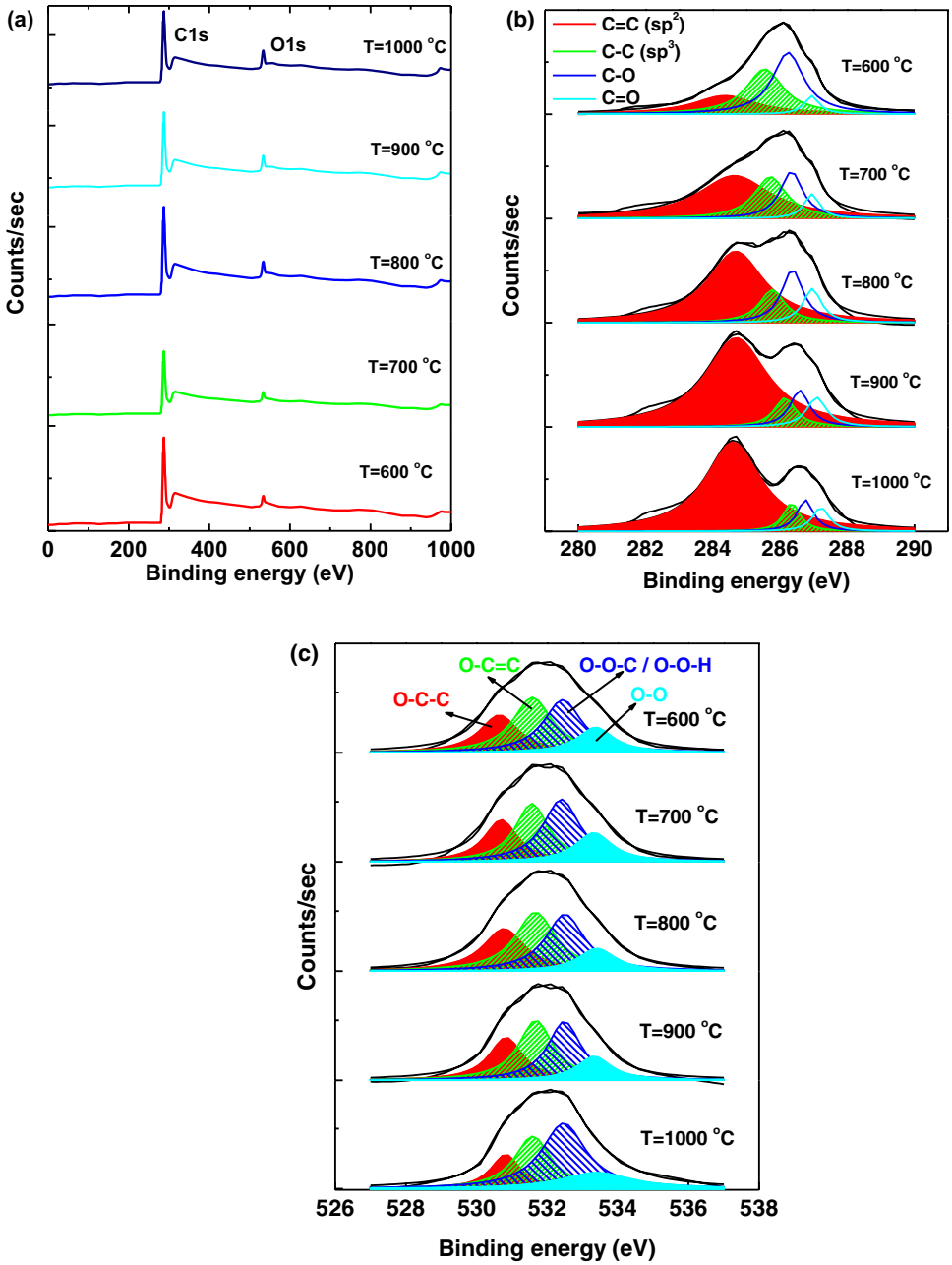

Fig. 4 **a** Full-scan XPS spectra of graphene samples **b** deconvolution of C(1 s) core orbital and **c** deconvolution of O(1 s) core orbital with varying the process temperature from 600 to 1000°C

where A_i is the area under the XPS curve and S_i is the relative sensitivity factor, which is 0.23 and 0.66 for C and O, respectively. The calculated values of atomic percentage for C and O are 96% and 4%, respectively, for the graphene sample synthesized at the process temperature of 1000 °C. The C/O ratio of all the samples are inserted in Table 2. No impurity atoms other than oxygen are present in the graphene sheets as obtained by the above XPS analysis. Figure 4b shows the deconvolution of C core orbital spectra of graphene with different process temperatures. For the proper analysis and better understanding, the C (1 s) core orbital is deconvoluted into four Lorentzian peaks. The binding energies at 284.35, 285.54, 286.24, 286.95 eV are assigned to the C=C(sp^2), C–C (sp^3), C–O and C=O, respectively (Vijapur et al. 2017). The XPS result is in accordance with the Raman results, indicating the presence of sp^3- and sp^2-hybridized C atoms in the graphene films. The major observations of deconvoluted C(1 s) core orbital are as follows:

1. The relative intensity of C=C (sp^2) and C–C (sp^3) shows an inverse relationship with each other. The intensity of C=C (sp^2) bond increased with the simultaneous decrease in the intensity of C–C (sp^3) bonds to increase in the process temperature. This indicates that the fraction of graphene increased with the reduction of three dimensional C structures for higher temperature pro-

cessed graphene samples. The increase in sp^2 bonds with the simultaneous decrease of sp^3 bonds indicates the purity of graphene at higher process temperature.

2. The relative intensity of the C–O bond decreases while that of the C=O bond increases with the increase in process temperature from 600 to 100 °C, indicating the formation of good-quality multilayer graphene sheets. The C–O bonds are expected to be the connector between two graphene layers, whereas the C=O are termed as the terminator in the grouping network. Therefore, the decrease in the C–O content indicates that by increasing the process temperature the O content is reduced in between two graphene layers.
3. A singlet peak is obtained for C(1 s) core orbital at 600 °C; however, the double-let peaks are observed in the process temperature above 800 °C. This is probably due to the increasing number of disorders during the restructurization of C structures of onion cells during the thermal exfoliation process taking place at higher temperatures.

Figure 4c shows the denconvolution of O peak in XPS spectra of graphene with the process temperature varying from 600 to 1000 °C to study the O environment in graphene layers. The O(1 s) core orbital is denconvoluted into four Lorentzian curves. The binding energies at 530.82, 531.59, 532.47, and 533.40 eV are assigned to O–C=C, O–C–C, O–O–C or O–O–H, and O–O bonds, respectively. The major observations obtained by the O(1 s) core orbital are (a) the width of O(1 s) core orbital decreased as the process temperature increased from 600 to 1000 °C, indicating the decrease in O content in the graphene layers. (b) The content of O–C–C (i.e., O attached with sp^3-hybridized C) and O–C=C (i.e., O attached with sp^2-hybridized C) bond decreased with the increase in process temperature from 600 to 1000 °C. (c) The relative intensity of O–O–H bond increased with the decrease in O–O bond intensity, with the process temperature increasing from 600 to 1000 °C. The observation mentioned above explains that the O content within the graphene layer decreased as the process temperature was raised from 600 to 1000 °C.

Figure 5a shows the cyclic voltammetric (CV) curve of graphene samples with different scan rates of 0.1 to 0.5V/s to analyze the electrochemical properties of graphene electrodes. The observed result showed that the CV curve of 600, 700, and 800 and 900 °C processed samples

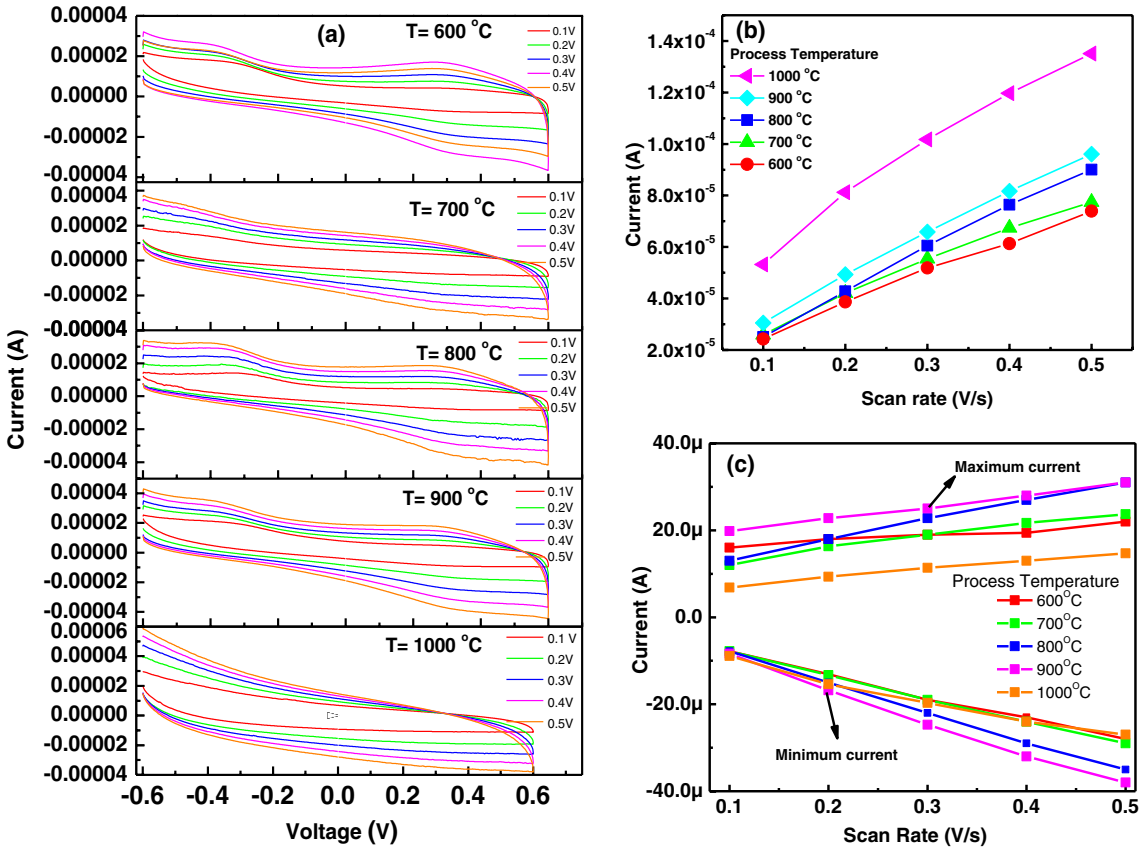

Fig. 5 **a** Cyclic voltammetric curve of graphene samples, **b** peak current versus scan rate plot of graphene samples with increasing process temperature from 600 to 1000°C

have quite distorted rectangular shape due to the oxidation reduction reaction taking place on the surface of graphene electrode as because of the presence of various oxygen-containing functional groups like carboxyl and hydroxyl organic groups within the graphene sheets. However, the CV loop processed of 1000 °C sample has a quasi-rectangular shape indicating quick charging–discharging responses to the applied voltage and formation of electrochemical double-layer capacitance (EDLC) due to the quality improvement of graphene sheets by the removal of oxygen-containing functional groups. The number of layers and its thickness have a great impact on the oxidation and reduction behavior of graphene, greater thickness of the samples leads to an increase in the oxidation and reduction currents. Moreover, the distorted hysteresis loop indicates the presence of pseudo capacitance whereas the quasi-rectangular shape indicates the double-layer capacitive behavior as reported earlier by Xu et al. (2011). As shown in Fig. 5a the two pairs of redox peaks of graphene samples having process temperature of 600, 800, and 900 °C arise at (±0.32 V), which is due to the transition between quinone or hydroquinone groups of carbon materials. Similar results were also obtained by Wan et al. and Hayes et al. for the graphene oxide materials (Wang et al. 2009; Hayes et al. 2015). The width of the hysteresis loop increased with increasing of process temperature from 600 to 1000 °C, indicating an increase in the porosity of the graphene samples. Figure 5b shows the area under the CV curve versus scan rate plot for the graphene samples processed at the temperature from 600 to 1000 °C. The integrated area of the CV curve increases with increasing the scan rate from 0.1 to 0.5V/s for all the graphene suggesting a good capacitive behavior due to the rapid charge propagation capability of double-layer capacitance for the graphene synthesized at 1000 °C. However, the pseudo-capacitive behavior is observed for the graphene samples prepared at 600, 700, 800, and 900 °C, indicating the stability of capacitance of the graphene electrodes (Purkait et al. 2018; Krishnamoorthy and Kim 2015). The areal capacitance of the as-prepared electrode was calculated from the C–V curves using the following equation:

$$C_{a}= \frac{I}{S\times \left[\frac{\mathrm{d}v}{\mathrm{d}t}\right]} \tag{5}$$

where C_a is the areal capacitance (F), I is the integrated area of the CV curve, dv/dt is the scan rate, S is the surface area of the electro active material. At the scan rate of 0.1V/s all the samples obtained a better capacitance value, which varies from 8.59×10^{-5}F/cm^2 to 18.8×10^{-5} F/cm^{2}with the process temperature varying from 600 to 1000 °C. By varying the scan rate from 0.1 V/s to 0.5V/s the capacitance decreased for graphene sample due to a decrease in the charge transfer rate through the electrochemical double layer formed at the interface between the electrode and the electrolyte. The capacitance of all the graphene samples with varying the scan rate from 0.1V/s to 0.5V/s is listed in Table 1.

Table 1 Areal capacitance of graphene samples in μF/cm^2 as obtained by the area of the CV curve

Process temperature °C	0.1 V/s	0.2 V/s	0.3 V/s	0.4 V/s	0.5 V/s
600	85.9	68.5	61.29	54.33	52.4
700	108.15	87.46	77.80	72.38	68.12
800	88.8	75.8	71.56	67.74	63.87
900	91.75	75.5	65.47	60.16	54.9
1000	188.6	144.0	120.2	105.65	95.7

Figure 5c shows the anodic and cathodic peak current versus the scan rate for the graphene electrodes with varying the process temperature from 600 to 1000 °C. For the 1000 °C processed graphene sample the middle portion of the CV curve was considered for obtaining the maximum and minimum current. Both of the anodic and cathodic peak current generated at (±0.32V) is linearly proportional to the scan rate ranging in between 0.1 and 0.5 V/s. The obtained plot reveals that the graphene samples show a good linear regression equation with correlation coefficients of $R^2=0.998$ and 0.993 for the anodic and cathodic peak, respectively. Hence, the overall electrochemical properties of graphene electrodes with H_2SO_4 are controlled by the surface-confined electrode process. Moreover, the peak-to-peak separation in the CV curve increases at higher sweep rates, suggesting a difficult charge transfer process at higher sweep rates (Devadas et al. 2012). The capacitance calculated from the CV curve is areal capacitance, which is not frequency dependent. As the carbon-to-oxygen ratio varies from 7.57 to 24.04 at % with an increasing process temperature of graphene, indicated the change of functional group with increase of process temperature. Therefore, the oxygen functional groups e.g., C–O and C=O/C–O–O– leading to reduction of conductivity of the graphene surface. This phenomenon has greater impact on the increasing of capacitance in graphene with increasing process temperature (He et al. 2018; Chen et al. 2017; Oh et al. 2014).

Figure 6 shows polarization curves of graphene samples through the Tafel plot by graphene-coated glassy carbon electrode. The polarization curves give information about the corrosion potential (E_{corr}) and corrosion current density (I_{corr}) of various electrodes. The values for E_{corr} and I_{corr} of graphene electrodes vary from −0.23 V to −0.12 V and −9.3 A/cm^2 to −9.1 A/cm^2, respectively, with the process temperature varying from 600 to 1000 °C. The shifting of corrosion potential values towards the more negative side with an increase in the corrosion current indicates an

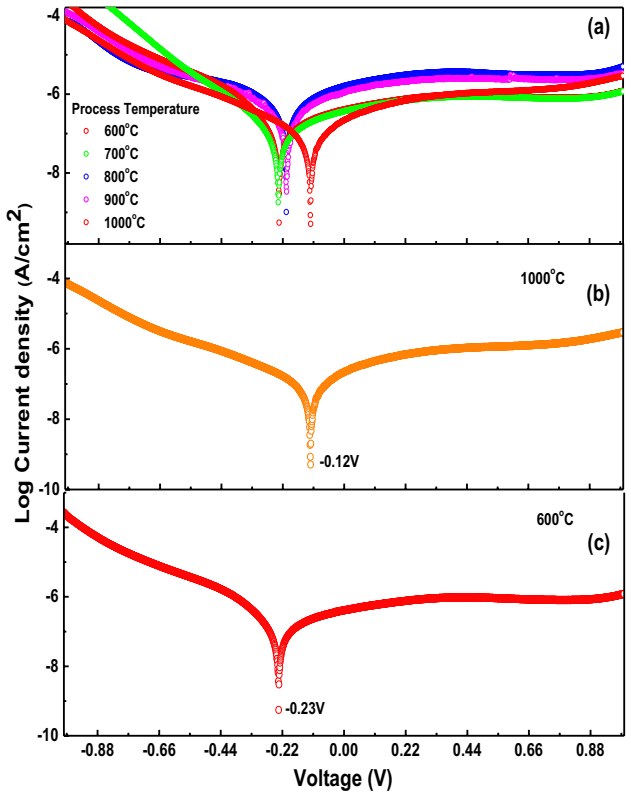

Fig. 6 **a** Tafel plot of all graphene samples processed at the temperature of 600–1000 °C, **b** Tafel plot for 1000 °C processed graphene and **c** Tafel plot for 600 °C processed graphene

increase in corrosion rate of the samples. This indicated that the graphene sample processed at 1000 °C is more corrosion-resistant as compared to the samples processed at lower temperatures at 600 °C.

To investigate the interfacial properties of graphene electrodes electrochemical impendence spectroscopy (EIS) has been performed for all graphene samples in the frequency range of 1–10^5Hz. Figure 7a shows the Nyquist plot of all the graphene samples with varying process temperature from 600 to 1000 °C, by taking *X*-axis as the real impedance *Z*′, and *Y*-axis as the negative imaginary impedance *Z*″. The inserted schematic equivalent circuit diagram inside the Fig. 7a represents, R_e as the resistance offered by the electrolytic solution, R_{CT} as the electron-transfer resistance of electrode and C_{dl} corresponding to the double-layer capacitance. The impedance diagrams obtained from the graphene samples show a semicircle, which corresponds to the electron-transfer resistance and the double-layer capacity (C_{dl}) of the film (Casero et al. 2012). As the process temperature increases from 600 to 1000 °C, the value of R_{CT} increases from 34.9 to 131.2 Ohm, indicating an increase in the electron transfer resistance (Su et al. 2018), which further reduces the electron-transfer process, hence the graphene sample processed at 600 °C is more suitable for the electro-catalytic activities. At very low frequency, the plot shows linear behavior due to the controlled diffusion process. From the Nyquist plot the capacitance of the interfacial reaction can be determined using the formula.

$$C_{dl} = \frac{\tau}{R_2} \tag{6}$$

where

$$\tau = \frac{1}{\omega_{max}} \tag{7}$$

where τ is the time constant and ω_{max} = frequency where the imaginary impedance is maximum. The time constant for the

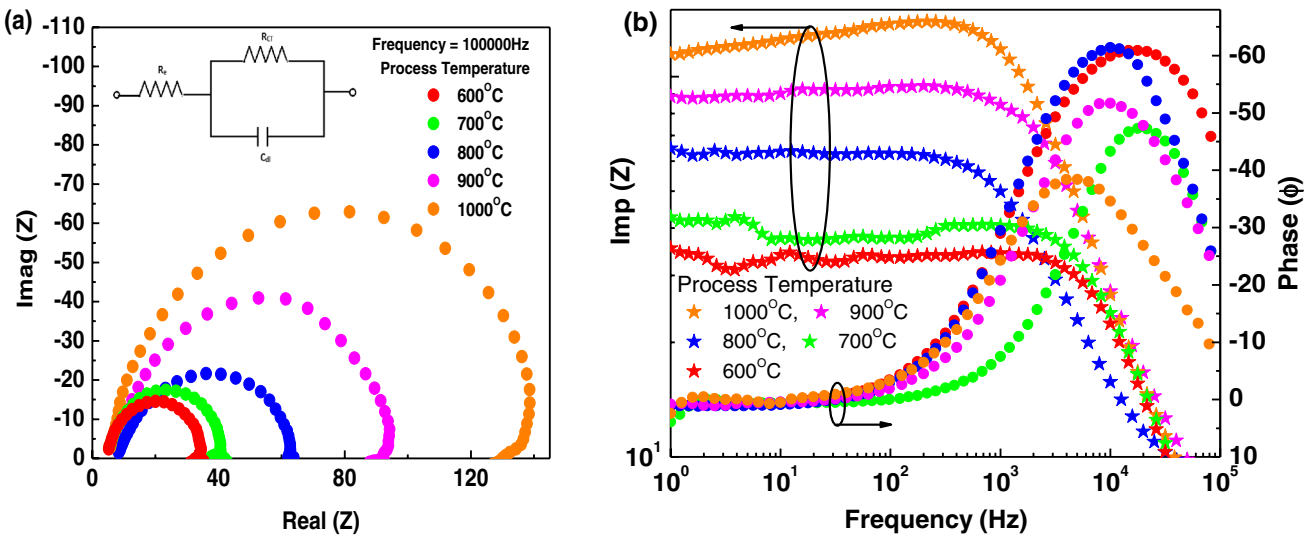

Fig. 7 **a** Nyquist plot and **b** Bode plot of graphene samples, by varying the process temperature from 600 to 1000 °C

diffusion process varies from 6.9×10^{-2} to 1.6×10^{-2} s and hence the value of specific capacitance of interfacial reaction varies from 19×10^{-4} to 1.2×10^{-4} F/cm^2 with increasing process temperature from 600 to 1000 °C.

Figure 7b shows the frequency responses of impedances of the graphene samples synthesized by varying the process temperature from 600 to 1000 °C. The result showed that the impedance increased from 35.31 to 116.30 Ohms as the process temperature increased from 600 to 1000 °C, respectively. The increase in impedance is due to the increase in the overall resistance ($R_e + R_{CT}$) offered by the graphene electrodes as the process temperature is increased from 600 to 1000 °C as listed in Table 2. The impedance at lower frequency region, i.e., below 10^3 Hz with the corresponding phase angle of ~ $\varphi = 0°$ gives the value of total resistance offered by the electrode and electrolyte $R_e + R_{CT}$. In the frequency range of 10^3 to 2×10^4 Hz with the corresponding maximum-phase angle, the value of impedance in this region is attributed to a capacitor in parallel with a resistance due to the charge transfer process (R_{CT}) for a reversible reaction as reported earlier by Casero et al. (2012). The estimated values of R_e and R_{CT} for all graphene samples at higher frequency region, i.e., $>10^5$ Hz are listed in Table 2. From the Bode plot as well minimum impedance was reflected by the 600 °C processed graphene sample with the R_e, R_{CT}, and φ_{max} values of 5.5 Ohm, 28.9 Ohm and −61.2°, respectively. As in Nyquist plot the frequency varied from 1 to 10^5 Hz, therefore, too much functional group hinders the transport of ions into the graphene surface. The strongly polarized oxygen functional groups also enhanced the hydrophilicity of the surface of the graphene surface, which is very beneficial for the rapid accumulation of ions on the electrode surface, but also reduces the mass transfer resistance (He et al. 2018; Chen et al. 2017; Oh et al. 2014). This is the main reason to reduce capacitance of bilayer in the graphene samples in the electrolytes.

Figure 8a shows the voltage-dependent impedance of graphene with different process temperature varying from 600 to 1000 °C. The impedance Z remains constant at positive voltages from 0 to 1 V; however, impedance increases with increasing negative voltage and maximum impedance was observed at −0.65 V. The impedance at −0.65 V decreased

Table 2 Different parameters obtained from Bode, Nyquist, Tafel, impedance-voltage plot and XPS analysis

	Bode plot			Nyquist plot				Tafel plot		Voltage dependent		C/O at. % (ratio)
	R_e (Ω)	R_{CT} (Ω)	φ_{max} in (°)	R_e (Ω)	R_{CT} (Ω)	ω_{max} (Hz)	C_{sp} (F/cm$^2\times10^{-4}$)	E_{corr} (V)	I_{Corr} (A/cm^2)	Z (Ω)	φ	
600 °C	5.5	28.9	−61.2	5.1	34.9	−14.5	19	−0.23	−9.3	15.79	−60.4	7.57
700 °C	5.6	34.8	−47.62	5.2	35.3	−17.3	16	−0.22	−8.7	10.9	−32.8	9.21
800 °C	8.3	53	−61.8	8.3	54.4	−21.86	8.4	−0.21	−9.0	7.15	−9.11	14.2
900 °C	7.6	87.1	−51.86	7.3	86.3	−40.83	2.8	−0.20	−8.45	7.4	−28.8	18.0
1000 °C	6.03	133.1	−38.6	5.7	131.2	−63.32	1.2	−0.12	−9.1	7.7	−35.8	24.04

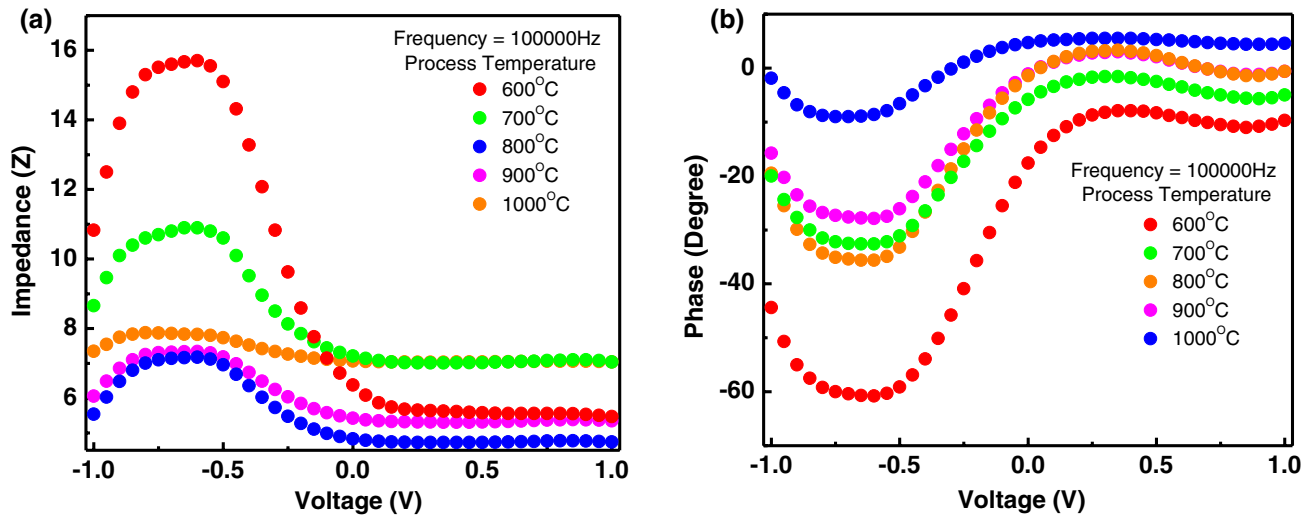

Fig. 8 **a** Impedance vs voltage and **b** phase vs voltage plot for graphene samples processed at various temperature of 600–1000°C

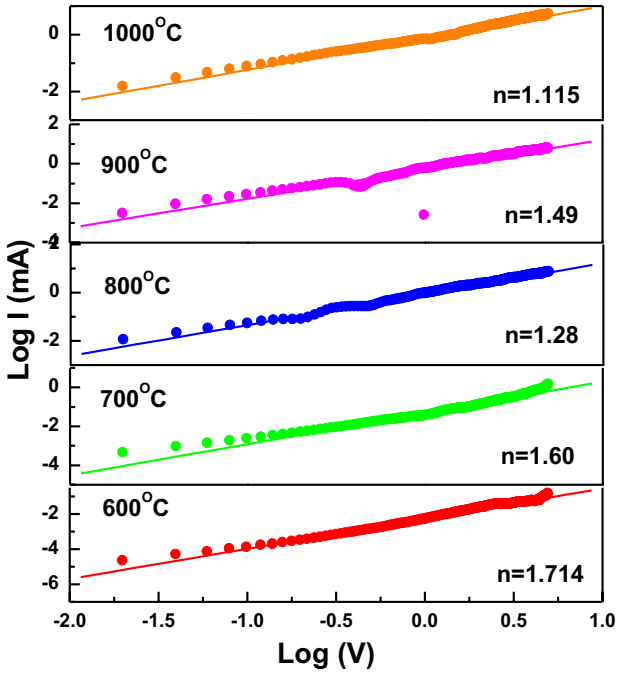

Fig. 9 Log *I* versus log *V* curve of graphene samples with varying the process temperature from 600 to 1000°C

from 15.79 to 7.7 Ohm with the process temperature increasing from 600 °C to 1000 °C. This indicates with the reverse voltage the diffusive charge accumulated at the interface of the electrode, hence, the relative capacitance and resistance increases with increase of voltage. The value of impedance increases from − 1 V and reaches a maximum of 15.79 Ohm at − 0.65 V indicating a decrease in the capacitive behavior, while at the negative side the value of impedance slowly decreases and becomes constant at 0 V indicating an increase in the capacitive behavior of graphene samples in this region.

Figure 8b shows the phase versus voltage plot of graphene electrodes within the voltage range of − 1 to 1V. The phase remained unchanged at 0–1 V whereas the phase changes at the negative potential between 0 and − 1 V. The maximum phase change is observed at − 0.65 V, which varies from − 60.4 to − 9.11° for the graphene samples with the process temperature changing from 600 to 1000 °C.

Figure 9 shows the log (*I*) versus log (*V*) characteristic curve of all the graphene samples with varying the process temperature from 600 to 1000°C. The ideality factor (*n*) value as evaluated from the log (*I*) versus log (*V*) curve decreases from 1.714 to 1.115 with increasing the process temperature from 600 to 1000 °C. The current (*I*) versus voltage (*V*) curves obtained for all graphene samples, follow the power law behavior where $I \infty V$. Similar studies were also done by Bhattacharya et al. for the graphene/$MoO_3$2D electrodes (Bhattacharya et al. 2015). The graphene samples synthesized at higher temperature approaches Ohmic behavior where $n = 1.115$, while the value of n increases and reaches up to $n = 1.714$ for 600 °C processed graphene sample. The increase of this ideality factor value is explained by the space-charge limited conduction (SCLC) mechanism. The low-temperature processed graphene samples contain more number of oxygen-containing functional groups attached to it, which further helps in trapping of different charges on its surface due to the presence of various dangling bonds. Therefore, the Ohmic behavior is observed for the low-temperature processed graphene samples.

Conclusion

Biomass synthesis of graphene was successfully done by the thermal exfoliation process of onion peels with varying the process temperature from 600 to 1000 °C. A transparent sheet-like structure is obtained for the graphene sample processed at 1000 °C with the layer thickness of 1.1 nm confirming the formation of bilayer graphene structure. An increase in the C/O atomic % ratio is observed from 7.57 to 24.04 for the graphene samples with the process temperature varying from 600 to 1000 °C indicating a decrease in the oxygen content for the graphene sample processed at higher temperature. The areal capacitance varied from 8.59×10^{-5} to 18.8×10^{-5} F/cm^2 for the scan rate of 0.1V/s with the process temperature varying from 600 to 1000 °C, showing maximum capacitance for the 1000 °C processed graphene samples. But a minimum corrosion rate was observed for the graphene sample processed at 1000 °C and having the E_{corr} and I_{corr}values of − 0.12 V and − 9.1 A/cm^2, respectively, therefore high-temperature processed graphene is a better corrosion-resistant material than the low-temperature processed ones. The AC impedance spectroscopy showed maximum impedance offered by the1000 °C processed graphene sample at the initial voltage of − 0.1 V. Moreover the log *I* versus log *V* curve showed that conduction in graphene is mainly favored by the SCLC conduction mechanism due to the presence of oxygen-containing functional groups.

Acknowledgements One of the authors Ms. Rabina Bhujel acknowledges Dr. RamdasPai and Mrs.Vasanthi Pai endowment fund for providing the financial support for conducting this research work.

Compliance with ethical standards

Conflict of interest The authors have no conflict of interest with anyone.

References

Akgül Ö, Alver Ü, Tanrıverdi A (2016) Calculation of electronic properties of multilayer graphene with Monte Carlo method. In: AIP Conf. Proc., vol 1722, pp 280001–280004

Andrea FC (2007) Raman spectroscopy of graphene and graphite: disorder, electron–phonon coupling, doping and nonadiabatic effects. Solid State Commun 143 : 47–57

Balasubramanian V, Selvakumari JC, Dhanalakshmi J, Ahila M, Padiyan DP (2018) Electrochemical analysis of graphene/Mo9Se11 nanocomposites towards energy storage application. J Mater Sci Mater Electron 29:7885–7892

Bharathidasan P, Kim DW, Devraj S, Shivakkumar SR (2016) Supercapacitive characteristics of carbon-based graphene composites. ElectrochemActa 204:146–153

Bhattacharya S, Dinda D, Saha K (2015) Role of trap states on storage capacity in a graphene/$MoO_3$2D electrode material. J Phys D Appl Phys 48:145303–145313

Bonanni A, Pumera M (2013) High-resolution impedance spectroscopy for graphene characterization. ElectrochemCommun 26:52–54

Casero E, Parra-Alfambra AM, Petit-Domínguez MD, Pariente F, Lorenzo E, Alonso C (2012) Differentiation between graphene oxide and reduced graphene by electrochemical impedance spectroscopy (EIS). ElectrochemCommun 20:63–66

Chen Y, Zhang Z, Huang Z, Zhang H (2017) Effects of oxygen-containing functional groups on the supercapacitor performance of incompletely reduced graphene oxides. Int J Hydrog Energy 42:7186–7194

Devadas B, Rajkumar M, Chen SM, Saraswathi R (2012) Electrochemically reduced graphene oxide/neodymium hexacyanoferrate modified electrodes for the electrochemical detection of paracetomol. Int J Electrochem Sci 7:3339–3349

EI-Kady MF, Shao Y, Kaner RB (2016) Graphene for batteries, supercapacitors and beyond. Nat Rev Mater 1:16033

Gao R, Hu N, Yang Z, Zhu Q, Chai J, Su Y, Zhang L, Zhang Y (2013) Paper-like graphene-Ag composite films with enhanced mechanical and electrical properties. Nanoscale Res Lett 8:32–40

Hao L, Li X, L.Zhi (2013) Carbonaceous electrode materials for supercapacitors. Adv Mater 25:3899–3904

Hayes WI, Joseph P, Mughal MZ, Papakonstantinou P (2015) Production of reduced graphene oxide via hydrothermal reduction in an aqueous sulphuric acid suspension and its electrochemical behavior. J Solid State Electrochem 19:361–380

He Y, Zhang Y, Li X, Lv Z, Wang X, Liu Z, Huang X (2018) Capacitive mechanism of oxygen functional groups on carbon surface in supercapacitors. Electrochim Acta 282:618–625

Jain R, Sinha A, N.Kumari AL, Khan (2016) A polyaniline/graphene oxide nanocomposite as a voltammetric sensor for electroanalytical detection of clonazepam. Anal Methods 8:3034–3045

Johra FT, Lee JW, Jung WG (2014) Facile and safe graphene preparation on solution based platform, J Ind Eng Chem 20 : 2883–2887

Krishnamoorthy K, Kim SJ (2015) Mechanochemical preparation of graphene nanosheets and their supercapacitor applications. J Indust Eng Chem 32:39–43

Latif IA, Merza SH (2016) Fabrication of functionalize reduce graphene oxide and its application in ampicillin detection. Nanosci Nanotech 6:24–33

Li Y, Yu C (2016) One-step electrosynthesis of graphene oxide-doped polypyrrole nanocomposite as a nanointerface for electrochemical impedance detection of cell adhesion and proliferation using two approaches. J Nanomater. https://doi.org/10.1155/2016/8932908 **(Article ID: 8932908)**

Lin X, Liang Y, Lu Z, Lou H, Zhang X, Liu S, Zheng B, Liu R, Fu R, Wu D (2017) Mechanochemistry: a green, activation-free and top-down strategy to high-surface-area carbon materials. ACS Sustain Chem Eng 5 : 8535–8540

Marcelina V, Syakir N, Wyantuti S, Hartati YW, Hidayat R, Fitrilawati F (2017) Characteristic of thermally reduced graphene oxide as supercapacitors electrode materials. In: IOP conf. series: mater sci eng, vol 196, pp 012034

N.Puri, SKMishra, A.Niazi AK, Srivastava, Rajesh (2014) Physicochemical characteristics of reduced graphene oxide based Pt-nanoparticles-conducting polymer nanocomposite film for immunosensor applications. J Chem Tech Biotech 90:1699–1706

Novoselov KS, Geim AK, Morozov SV, Jiang D, Zhang Y, Dubonos SV, Grigorieva IV, Firsov AA (2004) Electric field effect in atomically thin carbon films. Science 306:666–669

Oh YJ, Yoo JJ, Kim YI, Yoon JK, Yoon HN, Kim JH, Park SB (2014) Oxygen functional groups and electrochemical capacitive behavior of incompletely reduced graphene oxides as a thin-film electrode of supercapacitor. Electrochimica Acta 116:118–128

Pal H, Bhubn S, Kumar P, Mahapatra R, Chatterjee S (2018) Synthesis of flexible graphene/polymer composites for supercapacitor applications. JMEPEG 27 : 2668–2672

Pan H, Li J, Feng Y (2010) Carbon nanotubes for supercapacitors. Nanoscale Res Lett 5:654–668

Park HJ, Meyer J, Roth S, Skákalová V (2010) Growth and properties of few-layer graphene prepared by chemical vapor deposition. Carbon 48:1088–1094

Phan TB, Luong TT, Mai TX, Mai TTT, Pham TT (2016) Effect of nanostructured graphene oxide on electrochemical activity of its composite with polyaniline titanium dioxide. Adv Nat Sci Nanosci Nanotechnol 7:015016

Portales MV, LazoFraga AR, DíazGarcía AM, García-Zaldívar O, Barranco AP, A.Frutis MA (2018) Cyclic voltammetry and impedance spectroscopy analysis for graphene-modified solid-state electrode transducers. J Solid State Electrochem 22:471–478

Purkait T, Singh G, Kumar D, Singh M, Dey RS (2018) High-performance fexible supercapacitors based on electrochemically tailored three-dimensional reduced graphene oxide networks. Sci Rep 8:640(1–640(13)

Q.Ke JWang (2016) Graphene based materials for supercapacitor electrodes—a review. J Materiomics 2:37–54

Roy N, Leung KT, Pradhan D (2015) Nitrogen doped reduced graphene oxide based Pt–TiO_2nanocomposites for enhanced hydrogen evolution. J Phys Chem C 119:19117–19125

Shams SS, Zhang LS, Hu R, Zhang R, Zhu J (2015) Synthesis of graphene from biomass: a green chemistry approach. Mater Lett 161:476–479

Shearer CJ, Slattery AD, Stapleton AJ, Shapter JG, Gibson CT (2016) Accurate thickness measurement of graphene. Nanotechnology 27 : 125704–125714

Singal S, Srivastava Rajesh AK (2017) Electrochemical impedance analysis of biofunctionalized conducting polymer-modified graphene-CNTsnanocomposite for protein detection. Nano-Micro Lett 9:7

Skryshevsky VA, Milovanov SY, Gavrilchenko IV, Tiagulskyi SI, Rusavsky AV, Lysenko VS, Nazarov AN (2015) Impedance spectroscopy of single graphene layer at gas adsorption. Phys Status Solidi A 212:1941–1945

Su Q, Lu Y, Liu S, Zhang X, Lin Y, Fu R, Wu D (2018) Nanonetwork-structured yolk-shell FeS_2@C as high-performance cathode materials for Li-ion batteries. Carbon 140 : 433–440

Supriya S, Kumar S, Kar M (2016) Impedance spectroscopy studies in cobalt ferrite-reduced graphene oxide nanocomposite. In: AIP Conf. Proc., vol 1728, pp 020566–020569

Tuinstra F, Koenig JL (1970) Raman spectrum of graphite. J Chem Phys 53 : 1126–1130

Vijapur SH, Wang D, Ingram DC, Botte GG (2017) An investigation of growth mechanism of coal derived graphene films. Mater Today Commun 11:147–155

Wall M (2011) The Raman spectroscopy of graphene and the determination of layer thickness. Thermo Scientific Application Note: 52252. https://tools.thermofisher.com/content/sfs/brochures/AN52252_E%201111%20LayerThkns_H_1.pdf

Wang DW, Li F, Zhao J, Ren W, Ghen ZG, Tan J, Wu ZS, Gentle I, Lu GQ, Cheng HM (2009) Fabrication of graphene/polyaniline composite paper via in situ anodic electropolymerization for high-performance flexible electrode. ACS Nano 3:1745–1752

Wang H, Wang C, Matios E, Li W (2017) Critical role of ultrathin graphene films with tunable thickness in enabling highly stable sodium metal anodes. Nano Lett 17 : 6808–6815

Xu B, Sui S, Yue Z, Cao X, Zhang S, Hou G, Yang Y (2011) What is the choice for supercapacitors: graphene or graphene oxide? Energy Environ Sci 4:2826–2830

Yan K, Lee HW, Gao T, Zheng G, Yao H, Wang H, Lu Z, Zhou Y, Liang Z, Liu Z, Chu S, Cui Y (2014) Ultrathin two-dimensional atomic crystals as stable interfacial layer for improvement of lithium metal anode. Nano Lett 14 : 6016–6022

Yoon Y, Jo J, Kim S, Lee IG, Cho BJ, Shin M, Hwang WS (2017) Impedance spectroscopy analysis and equivalent circuit modeling of graphene oxide solutions. Nanomaterials 7:446

Zaaba NI, Foo KL, Hashim U, Tan SJ, Liu WW, Voon CH (2017) Synthesis of graphene oxide, using modified hummers method : solvent influence. Procedia Eng 184:469–477